15th Triennial World Congress, Barcelona, Spain

TRAJECTORY CONTROL OF CRANE LOAD POSITION AND INCLINATION

Harald Aschemann, Oliver Sawodny, Eberhard P. Hofer

Department of Measurement, Control and Microtechnology
University of Ulm, D-89069 Ulm, Germany
E-mail: harald.aschemann@e-technik.uni-ulm.de
Tel.: +49 731 5026336, Fax: +49 731 5026301

Abstract: A gain-scheduled trajectory control is exemplary presented for two of six available axes of an overhead crane that allows for positioning and inclining the crane load according to specified trajectories. Besides its tracking capabilities, the proposed control provides an active oscillation damping. The overall control structure consists of independent axis controllers, which are adapted to measurements of varying system parameters. These axis controllers take advantage of combined feedforward and feedback control as well as observer based disturbance rejection. The achieved control performance is shown by selected experimental results from an implementation on a 5 t - bridge crane. *Copyright @ 2002 IFAC*

Keywords: Trajectory control, gain scheduling, disturbance observer, crane control, robotics

1. INTRODUCTION

Until now, most papers concerning crane control have focussed on position control of the crane load in the three dimensional workspace ignoring the additionally three degrees of freedom as regards load orientation (Boustany and d`Andréa-Novel, 1992; Bryfors and Sluteij, 1996; Delaleau and Rudolph, 1998; Nguyen 1994). At the University of Ulm, a trajectory control concept for an overhead crane has been developed that focuses on the load motion and allows for trajectory control as well as active oscillation damping concerning all six load degrees of freedom. For this purpose, the crane has been upgraded with an orientation unit that is equipped with three additional axes, each actuated by an torque controlled DC-motor. By this, the capabilities of an automated overhead crane are extended considerably and, moreover, it can be considered as a robot manipulator that combines the capability of handling heavy loads with a large workspace. The overhead crane consists of six actuated axes (fig. 1). The *x*-, *y*- and *z*-axes allow for positioning of the crane load in the three dimensional workspace. The crane load can be hoisted or lowered in z-direction by means of the rope suspension. The *x*-axis represents the direction of the bridge motion, whereas the direction of the trolley motion on the bridge is referred to as *y*-axis.

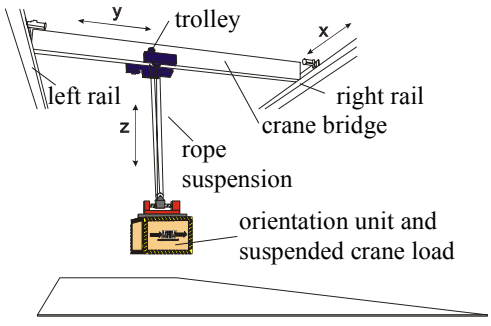

Fig. 1. Crane structure

The orientation unit with additionally three axes for orientating the crane load is equipped with two additional translational axes (*a*- and *b*-axis) and one rotational axis (*c*-axis) for the orientation around the *z*-axis, i.e. the rope suspension. In the sequel, both the *y*-axis and the according axis of the orientation unit, the *b*-axis, are regarded exemplary. This involves the derivation of an appropriate mathematical model, feedforward and feedback controller design as well as the design of disturbance observers to compensate for non-linear friction forces acting on the drives. The implementation of the proposed control at a 5 t - bridge crane is described in detail and measurement results taken from experiments at the bridge crane emphasise the efficiency of this control approach.

2. MULTIBODY MODEL OF THE CRANE

First, a central mathematical model for both crane axes under consideration shall be established. This common model is then used to derive a decentralised design model for each of these axes, i.e. the *y*-axis and the *b*-axis.

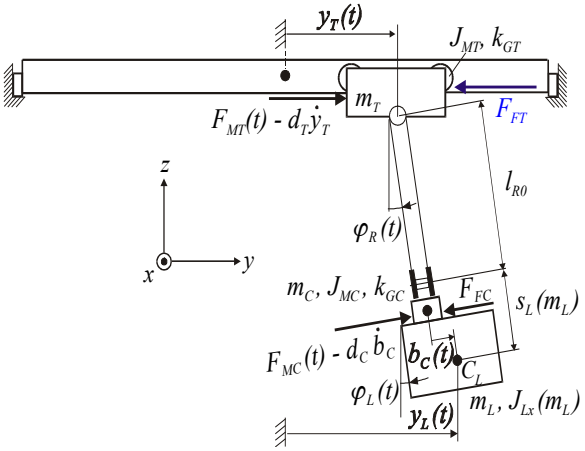

Fig. 2: Multibody model of the crane system

The motion of the mechanical system in *y*-direction is described by a multibody system consisting of three rigid bodies (fig. 2): the trolley (mass m_T, drive mass moment of inertia J_{MT}, resulting gear transmission ratio k_{GT}), the carriage of the orientation unit (mass m_C can be neglected, drive mass moment of inertia J_{MC}, resulting gear transmission ratio k_{GC}) and the crane load (mass m_L, mass moment of inertia J_{Lx}). The load center of gravity C_L shows an offset s_L in *z*-direction. The rope suspension is modelled as a massless rigid link with length l_{R0}. The kinematics of the mechanical system in *y*-direction can be described by four generalised coordinates: the position of the trolley $y_T(t)$, the rope angle $\varphi_R(t)$, the displacement of the carriage $b_C(t)$, and the orientation angle of the load $\varphi_L(t)$. The controlled variables are the position $y_L(t)$ of the load center of gravity and the orientation angle of the load $\varphi_L(t)$. By applying Lagrange's equations, non-linear equations of motion are computed in symbolic form. Under the assumption of both small rope angles and small load angles, the following linearised equations can be stated

$$\boldsymbol{M}\,\ddot{\boldsymbol{q}} + \boldsymbol{D}\,\dot{\boldsymbol{q}} + \boldsymbol{K}\,\boldsymbol{q} = \boldsymbol{f}_u + \boldsymbol{f}_e = \boldsymbol{F}_u\,\boldsymbol{u} + \boldsymbol{F}_e\,\boldsymbol{e}\,, \quad (1)$$

with the mass matrix (2)

$$\boldsymbol{M} = \begin{bmatrix} m_{11} & m_L l_{R0} & m_L & m_L s_L \\ m_L l_{R0} & m_L l_{R0}^2 & m_L l_{R0} & m_L l_{R0} s_L \\ m_L & m_L l_{R0} & m_L + J_{MC} k_{GC}^2 & m_L s_L \\ m_L s_L & m_L l_{R0} s_L & m_L s_L & m_L s_L^2 + J_{Lx} \end{bmatrix}$$

containing $m_{11} = m_T + J_{MT}\,k_{GT}^2 + m_L$,
the damping matrix

$$\boldsymbol{D} = diag\begin{pmatrix} d_T & 0 & d_C & 0 \end{pmatrix}, \quad (3)$$

the stiffness matrix

$$\boldsymbol{K} = \begin{bmatrix} 0 & 0 & 0 & 0 \\ 0 & m_L l_{R0}\, g & 0 & 0 \\ 0 & 0 & 0 & m_L g \\ 0 & 0 & m_L g & m_L s_L g \end{bmatrix}, \quad (4)$$

and the input matrices

$$\boldsymbol{F}_u = -\boldsymbol{F}_e = \begin{bmatrix} 1 & 0 & 0 & 0 \\ 0 & 0 & 1 & 0 \end{bmatrix}^T. \quad (5)$$

according to the control input $\boldsymbol{u} = [F_{MT} \quad F_{MC}]^T$ as well as the disturbance input $\boldsymbol{e} = [F_{FT} \quad F_{FC}]^T$, respectively. The symbolic mathematical model contains two system parameters with dominant variations during operation: the rope length l_{R0} and the load mass m_L, which are combined in the vector of varying system parameters $\boldsymbol{p} = [l_{R0} \quad m_L]^T$. To take these model variations into account, the gain scheduling technique is utilised. As the varying system parameters are available by direct measurements, the complete control structure can be adapted. With the usual choice of the state vector

$$\boldsymbol{x} = [\boldsymbol{q} \quad \dot{\boldsymbol{q}}]^T, \quad (6)$$

the state space representation becomes

$$\begin{bmatrix} \dot{\boldsymbol{q}} \\ \ddot{\boldsymbol{q}} \end{bmatrix} = \begin{bmatrix} \boldsymbol{0} & \boldsymbol{I} \\ -\boldsymbol{M}^{-1}\boldsymbol{K} & -\boldsymbol{M}^{-1}\boldsymbol{D} \end{bmatrix} \begin{bmatrix} \boldsymbol{q} \\ \dot{\boldsymbol{q}} \end{bmatrix} + \begin{bmatrix} \boldsymbol{0} \\ \boldsymbol{M}^{-1}\boldsymbol{F}_u \end{bmatrix} \boldsymbol{u} + \begin{bmatrix} \boldsymbol{0} \\ \boldsymbol{M}^{-1}\boldsymbol{F}_e \end{bmatrix} \boldsymbol{e}$$

or in abbreviated notation (7)

$$\dot{\boldsymbol{x}} = \boldsymbol{A}\,\boldsymbol{x} + \boldsymbol{B}_u\,\boldsymbol{u} + \boldsymbol{B}_e\,\boldsymbol{e}\,.$$

At this, the system matrix $\boldsymbol{A}$, the input matrices $\boldsymbol{B}_u$ and $\boldsymbol{B}_e$ of the control input $\boldsymbol{u}$ and the disturbances $\boldsymbol{e}$ are introduced, respectively.

3. DECENTRALISED DESIGN MODELS

The mechanical models that are used for the decentralised feedback control design of the *y*-axis and the *b*-axis are directly derived from the central design model by applying model reduction techniques. For each axis $q = y, b$ the vector of generalised coordinates $\boldsymbol{q}$ is expressed as a linear combination of gene-

ralised coordinates $\boldsymbol{q}_q$ and given reference motions $\boldsymbol{g}_q$ according to

$$\boldsymbol{q} = \boldsymbol{J}_q \boldsymbol{q}_q + \boldsymbol{g}_q , \qquad (8)$$

where $\boldsymbol{q}_q$ denotes the vector of generalised coordinates for the design model of reduced order. The corresponding time derivatives result in

$$\dot{\boldsymbol{q}} = \boldsymbol{J}_q \dot{\boldsymbol{q}}_q + \dot{\boldsymbol{g}}_q , \; \ddot{\boldsymbol{q}} = \boldsymbol{J}_q \ddot{\boldsymbol{q}}_q + \ddot{\boldsymbol{g}}_q . \qquad (9)$$

By inserting these expressions into the equations of motions, the reduced order equations of motion for the *q*-axis are obtained

$$\boldsymbol{M}_q \ddot{\boldsymbol{q}}_q + \boldsymbol{D}_q \dot{\boldsymbol{q}}_q + \boldsymbol{K}_q \boldsymbol{q}_q = \boldsymbol{f}_{qu} + \boldsymbol{f}_{qe} . \qquad (10)$$

The new system matrices are given by

$$\boldsymbol{M}_q = \boldsymbol{J}_q^T \boldsymbol{M} \boldsymbol{J}_q , \; \boldsymbol{D}_q = \boldsymbol{J}_q^T \boldsymbol{D} \boldsymbol{J}_q , \; \boldsymbol{K}_q = \boldsymbol{J}_q^T \boldsymbol{K} \boldsymbol{J}_q . \qquad (11)$$

The new control input is $\boldsymbol{f}_{qu} = \boldsymbol{J}_q^T \boldsymbol{f}_u$, whereas the new disturbance vector

$$\boldsymbol{f}_{qe} = \boldsymbol{J}_q^T \left[\boldsymbol{f}_e - \boldsymbol{M}\, \ddot{\boldsymbol{g}}_q - \boldsymbol{D}\, \dot{\boldsymbol{g}}_q - \boldsymbol{K}\, \boldsymbol{g}_q \right] \qquad (12)$$

consist of non-linear friction forces as well as coupling forces due to $\boldsymbol{g}_q$ and its first two time derivatives.

4. DECENTRALISED FEEDBACK CONTROL

The decentralised design model for the *b*-axis can be stated as

$$\boldsymbol{M}_b \ddot{\boldsymbol{q}}_b + \boldsymbol{D}_b \dot{\boldsymbol{q}}_b + \boldsymbol{K}_b \boldsymbol{q}_b = \boldsymbol{f}_{bu}\, u_b + \boldsymbol{F}_{be}\, \boldsymbol{e}_b . \qquad (13)$$

The new system matrices are given by

$$\boldsymbol{M}_b = \begin{bmatrix} m_L + J_{MC} k_{GC}^2 & m_L s_L \\ m_L s_L & J_{Lx} + m_L s_L^2 \end{bmatrix},$$

$$\boldsymbol{D}_b = \begin{bmatrix} d_C & 0 \\ 0 & 0 \end{bmatrix}, \; \boldsymbol{K}_b = \begin{bmatrix} 0 & m_L g \\ m_L g & m_L s_L g \end{bmatrix}, \qquad (14)$$

$$\boldsymbol{f}_{bu} = \begin{bmatrix} 1 \\ 0 \end{bmatrix}, \; \boldsymbol{F}_{be} = \begin{bmatrix} -1 & -m_L \\ 0 & -m_L s_L \end{bmatrix}.$$

The motor force of the carriage drive represents the control input $u_b = F_{MC}$, whereas the vector of disturbances $\boldsymbol{e}_b = [F_{FC} \quad \ddot{y}_S]^T$ consists of both the non-linear friction force F_{FC} acting on the carriage drive and the coupling acceleration of the rope suspension $\ddot{y}_S = \ddot{y}_T + l_{R0} \ddot{\varphi}_R$. The equations of motion are transformed into state space representation

$$\dot{\boldsymbol{x}}_b = \boldsymbol{A}_b \boldsymbol{x}_b + \boldsymbol{b}_{bu} u_b + \boldsymbol{B}_{be} \boldsymbol{e}_b , \qquad (15)$$

according to the state vector $\boldsymbol{x}_b = [\boldsymbol{q}_b \quad \dot{\boldsymbol{q}}_b]^T$. For control design the LQR approach based on the time weighted performance index

$$J = \frac{1}{2} \int_0^\infty \left(\boldsymbol{x}_b^T \boldsymbol{Q}_b \boldsymbol{x}_b + r\, u_b^2 \right) e^{2\alpha t}\, dt \qquad (16)$$

is employed, with the diagonal weighting matrix $\boldsymbol{Q}_b \geq \boldsymbol{0}$ and the scalar weighting factor $r_b > 0$. Using this time weighted criterion, the maximum real part $s = -\alpha$ of the resulting closed-loop poles can be specified. The corresponding linear feedback control law $u_{b,FB} = -\boldsymbol{k}_{b,FB}^T(m_{L,i})\, \boldsymbol{x}_b$, which contains the gain vector

$$\boldsymbol{k}_{b,FB}^T(m_{L,i}) = r_b^{-1}\, \boldsymbol{b}_{bu}^T(m_{L,i})\, \boldsymbol{P}(m_{L,i}) , \qquad (17)$$

is calculated with the solution $\boldsymbol{P}(m_{L,i})$ of the algebraic Riccati-equation (ARE) (18)

$$\boldsymbol{A}_{b\alpha}^T(m_{L,i})\, \boldsymbol{P}(m_{L,i}) + \boldsymbol{P}(m_{L,i})\, \boldsymbol{A}_{b\alpha}(m_{L,i}) - \boldsymbol{P}(m_{L,i})\, \boldsymbol{b}_{bu}(m_{L,i})\, r_b^{-1}\, \boldsymbol{b}_{bu}^T(m_{L,i})\, \boldsymbol{P}(m_{L,i}) + \boldsymbol{Q}_b = \boldsymbol{0} .$$

Here, the matrix $\boldsymbol{A}_{b\alpha} = \boldsymbol{A}_b + \alpha\, \boldsymbol{I}$ has to be utilised according to the chosen performance index. The solution of ARE $\boldsymbol{P}(m_{L,i})$ and, hence, the gain matrix $\boldsymbol{k}_{b,FB}^T$ are continuous if both the system matrices $\boldsymbol{A}_b$ and $\boldsymbol{b}_{bu}$ depend continuously on the load mass m_L and constant weightings are used, i.e. $\boldsymbol{Q}_b = \boldsymbol{const.}$ and $r_b = const.$ In order to allow for gain scheduling, the control design is performed for a specified number of operating points *i* representing the range of possible system parameter variation. Then, an approximated description is derived for this set of controller gains using look-up tables in combination with linear interpolation between the operating points. In fig. 3, the controller gain $k_{FB,1}(m_L)$ for the first state variable b_C is depicted exemplary.

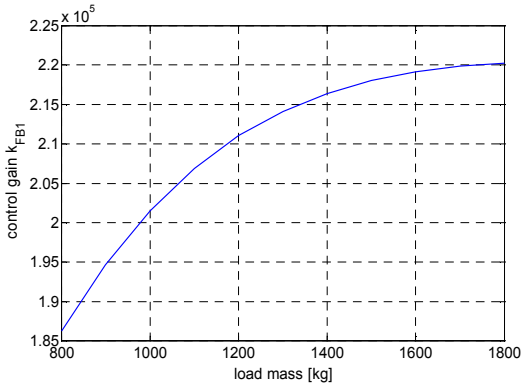

Fig. 3. Feedback control gain $k_{FB,1}(m_L)$ in dependence on the load mass m_L

To avoid hidden weightings, the elements of the diagonal matrix $\boldsymbol{Q}_b$ and r_b are divided by the squared maximum values of the according variables, respectively. The resulting closed-loop poles due to this gain-scheduled LQR design are variable in contrast to a gain scheduling based on a fixed pole configuration (Aschemann, *et al.*, 2000a). The control design for the *y*-axis is performed analogously and leads to the feedback control law $u_{y,FB} = -\boldsymbol{k}_{y,FB}^T(\boldsymbol{p})\, \boldsymbol{x}_y$, in which the vector $\boldsymbol{x}_y = [y_T \quad y_L \quad \dot{y}_T \quad \dot{y}_L]^T$ denotes the state vector and $y_L = y_T + (l_{R0} + s_L)\varphi_R$ represents the load position that is used for feedback.

5. CENTRAL FEEDFORWARD CONTROL

The central feedforward control action consists of both a linear part and a non-linear part. The linear feedforward control part provides the reference forces according to the linear system model and is calculated with the reference trajectory. Aim of the feedforward control design is an perfect tracking of specified trajectories for the controlled variables: the

load position in y-direction y_L as well as the load orientation φ_L. Both controlled variables are combined in the output vector (19)

$$\boldsymbol{y} = \begin{bmatrix} y_L \\ \varphi_L \end{bmatrix} = \boldsymbol{C}\,\boldsymbol{x} = \begin{bmatrix} 1 & l_{R0} & 1 & s_L & 0 & 0 & 0 & 0 \\ 0 & 0 & 0 & 1 & 0 & 0 & 0 & 0 \end{bmatrix} \boldsymbol{x},$$

where the matrix $\boldsymbol{C}$ describes the linear dependence on the state vector $\boldsymbol{x}$. For the central feedforward control part the following form has been chosen, where the index d denotes the decentralised parts on the diagonal and the index c stands for the central off-diagonal parts

$$\boldsymbol{u}_{LF} = \begin{bmatrix} u_{y,LF} \\ u_{\varphi,LF} \end{bmatrix} = \begin{bmatrix} \boldsymbol{k}_{yd}^T & \boldsymbol{k}_{yc}^T \\ \boldsymbol{k}_{bc}^T & \boldsymbol{k}_{bd}^T \end{bmatrix} \begin{bmatrix} \boldsymbol{w}_y \\ \boldsymbol{w}_\varphi \end{bmatrix}. \qquad (20)$$

It represents a linear combination of all reference values and its first four time derivatives, which are combined in the reference vectors (21)

$$\boldsymbol{w}_y = \left[y_{L,ref} \quad \dot{y}_{L,ref} \quad \ddot{y}_{L,ref} \quad \dddot{y}_{L,ref} \quad y_{L,ref}^{(IV)} \right]^T,$$

$$\boldsymbol{w}_\varphi = \left[\varphi_{L,ref} \quad \dot{\varphi}_{L,ref} \quad \ddot{\varphi}_{L,ref} \quad \dddot{\varphi}_{L,ref} \quad \varphi_{L,ref}^{(IV)} \right]^T.$$

Alternatively, this feedforward control law can be expressed in the frequency domain using a transfer function matrix

$$\boldsymbol{u}_{LF} = \boldsymbol{G}_{LF}(s) \begin{bmatrix} y_{L,ref} \\ \varphi_{L,ref} \end{bmatrix}. \qquad (22)$$

By rewriting both decentralised feedback control laws in dependence on the state vector $\boldsymbol{x}$

$$\boldsymbol{u}_{FB} = \begin{bmatrix} u_{y,FB} \\ u_{b,FB} \end{bmatrix} = -\boldsymbol{K}_{FB}\,\boldsymbol{x} \qquad (23)$$

the command transfer function matrix becomes (24)

$$\boldsymbol{G}(s) = \boldsymbol{C}(s\boldsymbol{I} - \boldsymbol{A} + \boldsymbol{B}_u \; \boldsymbol{K}_{FB})^{-1} \boldsymbol{B}_u \; \boldsymbol{G}_{LF}(s)$$

The feedforward gain vectors $\boldsymbol{k}_{ij}^T = \boldsymbol{k}_{ij}^T(\boldsymbol{p})$, which depend on the varying system parameters $\boldsymbol{p}$, can be calculated in symbolic form by applying the final value theorem of the Laplace transform to the elements of $\boldsymbol{G}(s)$. Up to the fourth time derivative of the reference trajectory, ideal tracking behaviour is aimed at for the diagonal elements, whereas ideal decoupling is aimed at for the off-diagonal elements (Aschemann, *et al.*, 2000b).

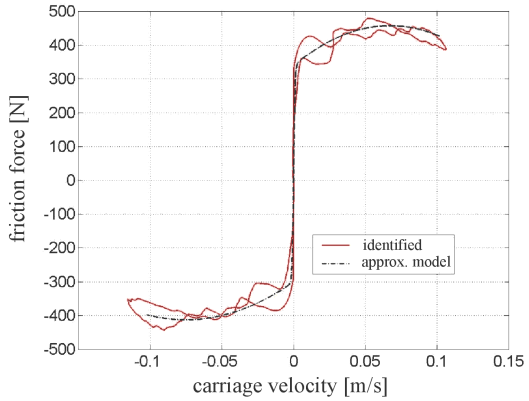

Fig. 4. Identified friction characteristic and non-linear friction model of the *b*-axis

The non-linear feedforward control part is dedicated to provide an open-loop compensation for the non-linear friction forces. The identified non-linear friction characteristic and an approximating friction model are shown in fig. 4 for the *b*-axis, exemplary.

The non-linear feedforward control part for the *b*-axis is given by the non-linear friction model $u_{b,NF} = F_{FC} = F_{FC}(\dot{b}_{C,ref})$ evaluated with the reference velocity of the *b*-axis. This reference velocity can be derived in symbolic form from the linear feedforward control part. It results in a linear combination of the reference vectors $\boldsymbol{w}_y$ and $\boldsymbol{w}_\varphi$. (25)

$$\dot{b}_{C,ref} = \left[0 \;\; 0 \;\; 0 \;\; -\frac{s_L}{g} \;\; 0 \;\Big|\; 0 \;\; -s_L \;\; 0 \;\; \frac{J_{Lx}}{m_L\, g} \;\; 0 \right]^T \begin{bmatrix} \boldsymbol{w}_y \\ \boldsymbol{w}_\varphi \end{bmatrix}$$

The non-linear friction model $F_{FT} = F_{FT}(\dot{y}_{T,ref})$ of the *y*-axis is evaluated with the reference trolley velocity $\dot{y}_{T,ref}$.

6. DISTURBANCE OBSERVER DESIGN

As the friction characteristics depend on lots of factors and may change during operation time, the non-linear feedforward control part cannot achieve a perfect disturbance rejection. Therefore, additional measures are necessary to cope with changeable friction characteristics. For this purpose, a reduced order disturbance observer is employed for each axis. In the following, the design approach is presented at the example of the *b*-axis. As disturbance model for the friction force F_{FC} an integrator model has proved advantageous, i.e. $\dot{F}_{FC} = 0$ (Aschemann, *et al.*, 2000 a, b). Since all state variables are forthcoming, the measurement vector of the observer is identical to the state vector $\boldsymbol{y}_{bB} = \boldsymbol{x}_b$. The input vector of the observer $\boldsymbol{u}_{bB} = [u_{bO,lin} \quad \ddot{y}_S]^T$ consists of the control input $u_{bO,lin} = u_{b,FB} + u_{b,LF} + u_{b,DC}$ except the non-linear feedforward part and the acceleration of the load suspension $\ddot{y}_S$. The state space representation of the reduced observer is given by (26)

$$\dot{\rho} = a_\rho\, \rho + \boldsymbol{b}_y^T\, \boldsymbol{y}_{bB} + \boldsymbol{b}_u^T\, \boldsymbol{u}_{bB}, \quad \hat{F}_{FC} = \rho + \boldsymbol{h}_b^T\, \boldsymbol{y}_{bB}$$

At this, the observer gain vector

$$\boldsymbol{h}_b^T = [0 \quad 0 \quad h_3 \quad 0]^T, \qquad (27)$$

the scalar system matrix

$$a_\rho = h_3 \cdot (J_{Lx} + m_L s_L^2) / n_a \text{ with}$$

$$n_a = m_L J_{Lx} + J_{MC}\, k_{GC}^2 \cdot (J_{Lx} + m_L s_L^2), \qquad (28)$$

and the input vectors

$$\boldsymbol{b}_u^T = \left[-\frac{(J_{Lx} + m_L s_L^2) h_3}{n_a} \quad \frac{m_L J_{Lx}\, h_3}{n_a} \right], \qquad (29)$$

$$\boldsymbol{b}_y^T = \left[-\frac{h_3\, m_L^2\, s_L g}{n_a} \quad \frac{J_{Lx} m_L g\, h_3}{n_a} \quad \frac{(J_{Lx} + m_L s_L^2) \cdot (h_3 + d_C)\, h_3}{n_a} \quad 0 \right]$$

concerning measurement vector $\boldsymbol{y}_{bB}$ and observer input $\boldsymbol{u}_{bB}$ are introduced, respectively. The observer dynamics can be specified by pole placement. By proposing a closed-loop characteristic polynomial $s+\alpha_0 = 0$, the observer gain h_3 results in

$$h_3 = -\frac{\alpha_0\, n_a}{(J_{Lx} + m_L s_L^2)} \,. \tag{30}$$

The estimated friction force $\hat{F}_{FC}$ can be directly applied to the carriage drive, i.e. $k_{b,DC} = 1$. Hence, the observer based disturbance compensation results in

$$u_{b,DC} = k_{b,DC}\hat{F}_{FC} = \hat{F}_{FC} \,. \tag{31}$$

7. CONTROLLER IMPLEMENTATION

The trajectory control scheme is shown in fig. 5 for the *b*-axis, exemplary. The complete control law for the *b*-axis

$$u_b = u_{b,LF} + u_{b,NF} + u_{b,FB} + u_{b,DC} \tag{32}$$

represents the sum of linear feedforward $u_{b,LF}$, non-linear feedforward $u_{b,NF}$, linear state feedback $u_{b,FB}$, and observer based disturbance compensation $u_{b,DC}$. The corresponding motor torque u_{bM} is obtained by premultiplying with the inverse gain transmission ratio, i.e. $u_{bM} = k_{GC}^{-1}\, u_b$. Note that all subsystems are adapted to the measured parameter vector $\boldsymbol{p}$. The carriage position b_C is measured by an encoder. The load angle φ_L is obtained as the sum of the small angular rope deflection at the trolley and the relative angular deflection between rope and orientation unit, which both are measured by incremental encoders.

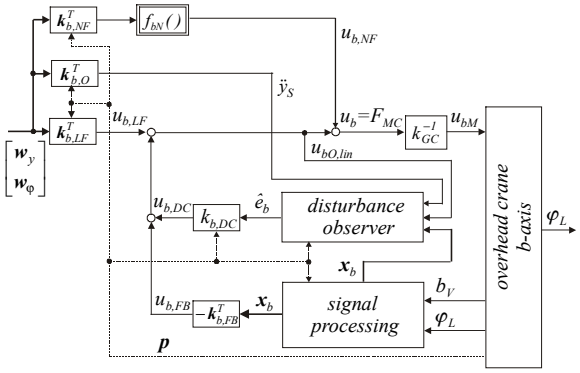

Fig. 5. Trajectory control scheme for the *b*-axis

8. EXPERIMENTAL RESULTS

The efficiency of the proposed control scheme shall be shown by measurements at a 5 t – bridge crane. At first, trajectory tracking concerning the *b*-axis with deactivated remaining axes is considered. The reference trajectory for the *b*-axis consists of a movement from $\varphi_L = 0°$ to $\varphi_L = 6°$, an 10 seconds break, and the return movement to $\varphi_L = 0°$.

As can be seen in the upper part of fig. 6, the feedforward disturbance rejection works quite well. Moreover, a further reduction of the tracking error as depicted in the lower part of fig. 6 can be achieved by additional use of a disturbance observer.

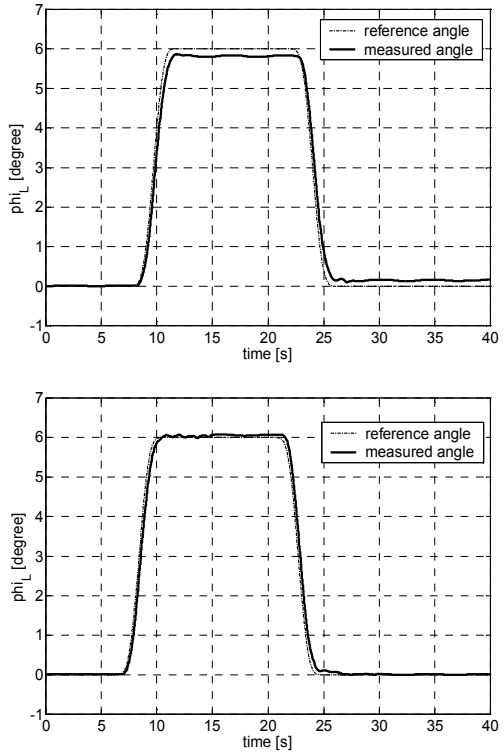

Fig. 6. Reference and measured load angle without (upper part) and with (lower part) observer based disturbance compensation for m_L=800 kg

In the following figures, a reference trajectory is tracked with the *y*-axis, while the *b*-axis should keep its reference value identical to zero, i.e. $\varphi_{L,ref} \equiv 0$. During the specified motions of the trolley by 2 m, the acceleration of the rope suspension $\ddot{y}_S$ acts as a disturbance on the *b*-axis control. Fig. 7 and 8 provide a comparison of reference values and measured values for both controlled variables: the load position y_L and the load inclination φ_L.

In fig. 7, measurement results are shown for a pure decentralised feedforward control, where the *b*-axis feedforward control is exclusively calculated with the reference $\boldsymbol{w}_\varphi$ and the *y*-axis feedforward control is solely based on the reference $\boldsymbol{w}_y$. The tracking behaviour concerning the load position is quite well with maximum deviations of less than 6 cm but the load angle φ_L shows maximum deviations of about 2° from its reference value zero. Steady-state accuracy is about 1 cm for the load position and about 0.3° for the load inclination.

In fig. 8, measurement results are presented for the same reference motion as in fig. 7, but now with the complete feedforward control as described in chapter 5. It is obvious that the compensation of the coupling forces leads to a reduction of the tracking error of the *b*-axis by approximately factor four with deviations of about 0.5°. The remaining oscillations with an

amplitude of approximately 0.2° can be tolerated from a practical point of view.

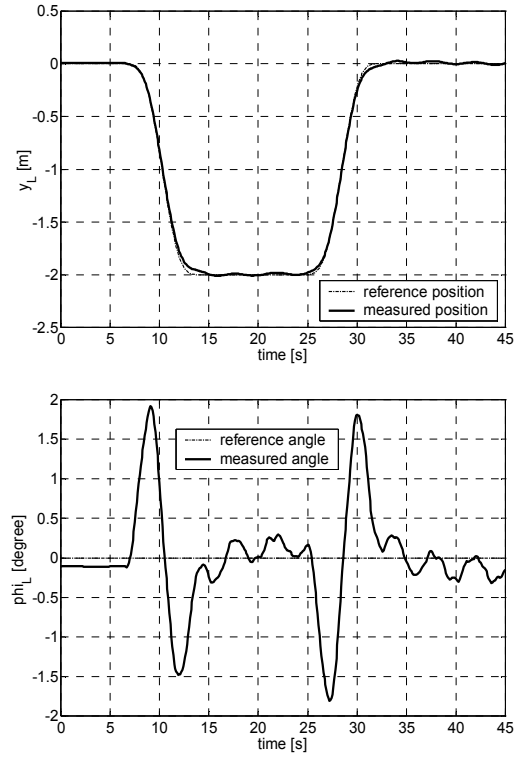

Fig. 7. Comparison of reference and measured controlled variables for m_L = 930 kg, l_R = 4.85 m with decentralised instead of central feedforward control

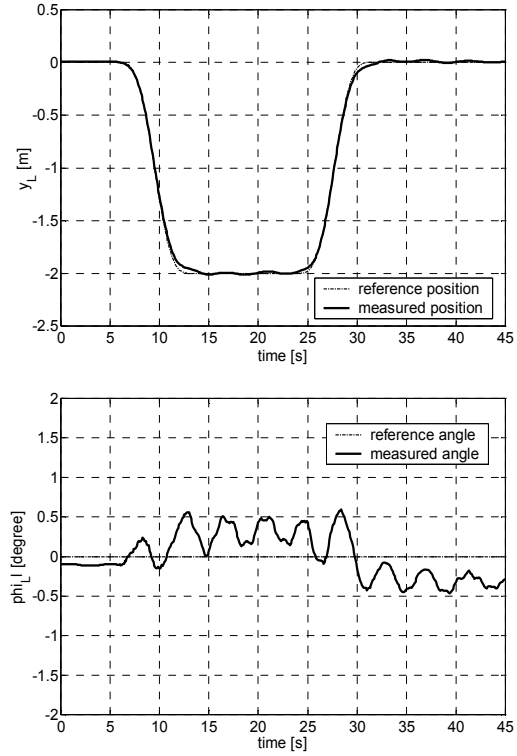

Fig. 8. Comparison of reference and measured controlled variables for m_L = 930 kg, l_R = 4.85 m with central feedforward control

9. CONCLUSION

A trajectory control approach is presented for the load position as well as the load inclination of an overhead crane, which has been upgraded with an additional orientation unit. Based on a multibody model of the crane, feedback and feedforward controllers as well as disturbance observers are derived in symbolic form. This allows for an adaptation of the complete control structure using the gain scheduling technique with respect to the varying system parameters rope length and load mass. Measurements, taken at a 5 t – bridge crane, show the benefits of the proposed control scheme as regards control performance and steady-state accuracy. Concerning the load position the achieved tracking error remains below 6 cm with a steady-state error less than 1 cm. The tracking error with respect to the load inclination is about 0.6° with a steady-state error of about 0.3° in the case of coupling force compensation using central feedforward control.

REFERENCES

Aschemann H., Sawodny O., Lahres S., Hofer E.P. (2000a). Disturbance Estimation and Compensation for Trajectory Control of an Overhead Crane. In: *Proceedings of American Control Conference ACC 2000*, Chicago, USA, pp. 1027 – 1031

Aschemann H., Sawodny O., Hofer E.P. (2000b). Active Damping of Tilt Oscillations and Trajectory Control of Overhead Cranes. Proceedings of IEEE Conference on Industrial Electronics, Control, and Instrumentation IECON 2000, Nagoya, Japan, pp. 70 – 75

Boustany F., d`Andréa-Novel B. (1992). Adaptive Control of an Overhead Crane using Dynamic Feedback Linearization and Estimation Design. In: *Proceedings of the 1992 IEEE International Conference on Robotics and Automation*, Nice, France, pp. 1963 – 1968

Bryfors, U., Sluteij, A. (1996). Integrated Crane Control. In: *Proceedings of the 16th Conference on Transportation Systems*, Zagreb, Croatia, pp. 167 – 171

Delaleau, E., Rudolph, J. (1998). Control of flat systems by quasi-static feedback of generalized states. In: *International Journal of Control*, **Vol. 71**, No. 5, pp. 745 – 765

Nguyen, H.T. (1994). State Variable Feedback Controller for an Overhead Crane. In: *Journal of Electrical and Electronics Engineering*, Australia, **Vol. 14**, No. 2, pp. 75 – 84